

January 29, 2021

Dr. Nathaniel E. Putzig, Senior Scientist
Planetary Science Institute
1546 Cole Blvd #120
Lakewood, CO 80401

RE: Project report, eastern Deuteronilus Mensae SHARAD 3D pilot study

Dear Than,

Enclosed is a short report describing the 3D processing work and results for the eastern region of Deuteronilus Mensae selected for the MRO-funded pilot project. Please don't hesitate to contact me with questions, revision suggestions, and/or comments.

Sincerely,

A handwritten signature in black ink, appearing to read 'Frederick J. Foss, II', written in a cursive style.

Frederick J. Foss, II, Founder & Principal
Freestyle Analytical & Quantitative Services, LLC

Executive Summary

At the end of July 2020, the MRO mission approved funding of a pilot project to perform so-called “advanced” 3D imaging using 467 SHARAD observations collected within the 25°-35°E, 37°-47°N area of eastern Deuteronilus Mensae (DM). Beyond producing the first such image within this specific region, the broader purpose of this project was to determine whether or not, and if so to what degree, the existing SHARAD coverage within heavily targeted mid-latitude regions supports 3D imaging. By mid-September 2020, colleagues at Planetary Science Institute (PSI) and Smithsonian Institution (SI) had generated and delivered all of the required input data, the preparatory 2D and 3D processing taking place over the ensuing 2 ½ months culminating with delivery of a DM 3D image at the beginning of December 2020. Preliminary visualization and analysis indicates that, while there are some expected processing artifacts due to insufficient coverage particularly in the cross-track direction, unprecedented 3D views of the DM subsurface are provided by the 3D image, affirming that the existing SHARAD coverage does indeed support 3D imaging and continued targeting and observation will serve to further improve any subsequent SHARAD 3D images of this area as well as others within the mid-latitudes. This report briefly describes the “advanced” 3D data processing methodology, presents results of its use to image the DM data in 3D, and concludes with recommendations for extending this work.

Introduction and Motivation

Roughly two years ago, discussion began about generating small (compared with polar) SHARAD 3D images of heavily targeted mid-latitude areas on Mars in support of the effort to better delineate the distribution of shallow subsurface water ice in these regions, to inform our understanding of both the glaciation history and water ice resources distribution in such areas. A natural question at the outset was “is the observational coverage sufficient to support 3D imaging?” In order to answer this question, at least for surface topography, a simple formula depending on SHARAD frequency, surface slope magnitude and “aspect” (i.e. azimuth relative to the observational azimuth) was used to define the along-track and cross-track sampling limits above which returns from the surface at a given location alias during sounding. Within the DM area, at regularly spaced locations along the various SHARAD orbits, actual along-track and cross-track radargram frame spacing was quantitatively compared with these corresponding aliasing limits and maps were generated showing coverage deficiencies. As the along-track spacing during sounding is almost certainly adequate to properly sample the surface (and subsurface) returns, we focused our attention on the cross-track spacing. Figure 1 shows the cross-track coverage deficiency map within DM (as of mid-February 2020), the pilot study area delineated within the magenta box. For most of DM, the cross-track coverage deficiency is at most a single observation needed between existing adjacent observations (represented by low-contrast grey dots against the grey THEMIS IR background), which continues to be addressed with further targeting and sounding. Proper sampling of the steeper slopes requires more infill observations (indicated in the map legend by warmer-colored dots corresponding to increasing numbers of infill observations required to eliminate the deficiency). In the vicinity of the steepest landform slopes, the cross-track coverage deficiency is largest (10 or more observations represented by red dots), likely too large to completely infill with additional observations. It is

likely, however, that returns from these steepest slopes (e.g. the walls of tall mesas or craters) are never recorded simply because the orbital acquisition geometry doesn't permit it, a problem that increase coverage density won't solve. This map increased confidence that a scientifically viable SHARAD 3D image could be produced using existing coverage despite coverage deficiencies proximal to landforms with the most topographic relief.

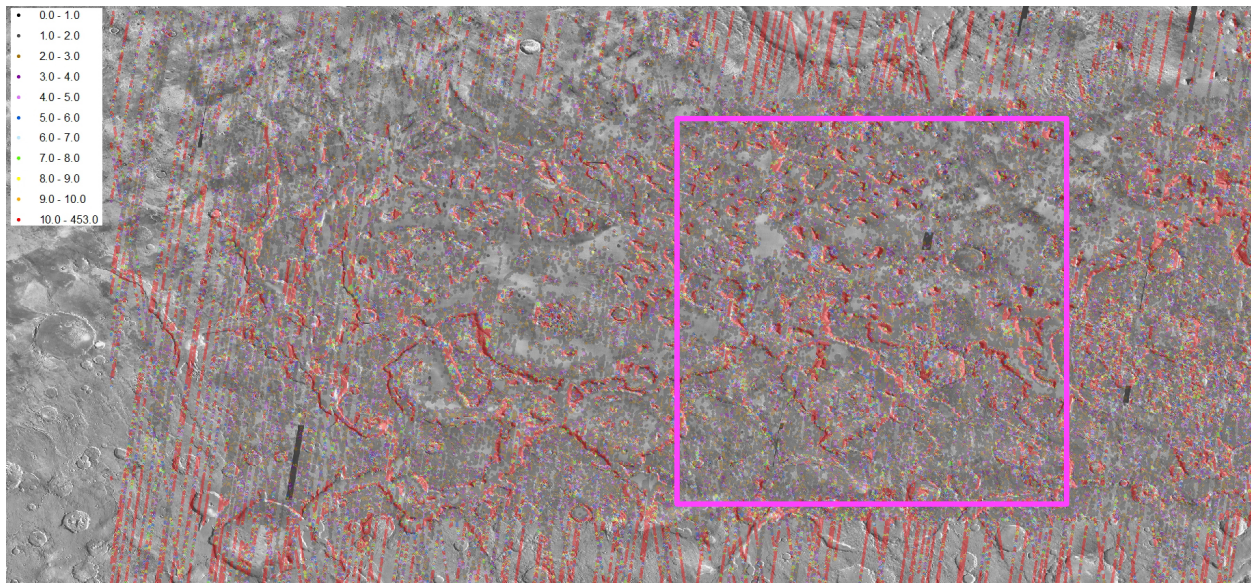


Figure 1. SHARAD cross-track coverage deficiency map of Deuteronilus Mensae region of Mars, the pilot study area within the magenta box. Grey-colored dots along the existing SHARAD observations indicate at most a single infill observation is required to sample the surface topography without aliasing. According to the legend, warmer-colored dots indicate more infill required between existing observations to properly sample the surface topography, with red dots indicating at least 10 infill observations required to sample the surface topography without aliasing. As expected, the red dots cluster around mesa and crater walls where slopes are largest.

“Advanced” 3D Processing Methodology

In April 2016, NASA selected and funded an ongoing MDAP project to perform so-called “advanced” 3D imaging of Planum Boreum (PB) using SHARAD data. The methodology used in that project is detailed in the Science/Technical/Management portion of the Putzig’s 2015 MDAP proposal, and both revises and extends the methodology used in two prior MDAP projects which resulted in the first SHARAD 3D images of PB and Planum Australe (PA) detailed in two final project reports and in Foss et al. (2017). Briefly, the “advanced” 3D methodology entails:

1. Generation and delivery of SHARAD radargrams in SEG-Y format, SAR processed with an improved ionosphere phase distortion correction algorithm (need reference) and a wider Doppler bandwidth, along with required ancillary data.
2. Generation and delivery of SHARAD surface clutter simulations (Choudhary et al. 2016) in SEG-Y format, co-located and consistent with corresponding radargrams, along with required ancillary data.
3. Import SEG-Y formatted radargrams and surface clutter simulations, generate/append 2D geometry, convert the dB power sample values in both radargrams and surface clutter simulations to so-called *reflection strength* which is simply the square root of power.

4. Derivation of “raw”, and subsequent application of median-smoothed versions of, differential time shifts required to co-register radargrams so that their surface return delay times closely match corresponding simulated surface return delay times. This step is critical for improving the delay time consistency and coherency of the entire collection of radargrams in 3D.
5. Preparatory 2D pre-processing of each radargram, including
 - a. Re-datuming the radargrams from their common final SAR processing datum (10,118.0 m above the Mars areoid) back to their individual orbit datums,
 - b. De-migrating the radargrams to approximately reverse the along-track range migration performed during SAR processing,
 - c. Re-datuming the radargrams from their individual orbit datums to a common constant average orbit radius datum,
 - d. Bulk shifting the radargrams to the maximum areoid radius found within the entire set of input radargrams to save storage space. The maximum areoid radius is also used as the reference surface for downward continuation of the 3D volume).
 - e. Output the radargrams in SEG-Y format with all header information needed for 3D processing.
6. Build the 3D geometry and information databases and assign the 3D geometry to the 3D prepared radargrams. In particular, assign the data to square spatial bins with spacing roughly matching that of the along-track frame spacing.
7. Sort the radargram frames by spatial bin number and their distance from the bin center.
8. Derive and apply intra-bin residual differential time delay shifts (so-called *trim statics*) to align frames within the bin prior to horizontal stacking of frames within the bin.
9. Apply observation-dependent gain correction factors to compensate for gain variations induced by MRO solar array (SA) and high gain antenna (HGA) position variations as described in Campbell et al. (2021, to appear). Note that this step was omitted for this pilot project (see QC discussion hereafter).
10. Stack the frames, normalizing the stacked sample amplitudes by the frame count, within the same spatial bin. Note that for this pilot project, this step was not performed prior to the next step, rather the pre-stack data was interpolated and regularized directly.
11. Spatially interpolate and regularize the frames within the 3D (stack) volume.
12. 3D downward continue (DC) the interpolated/regularized 3D stack volume from the common average orbit radius datum to the maximum areoid radius datum.
13. 3D migrate the 3D DCed volume using pure water ice velocity.
14. Use the appropriately re-datumed nadir surface delay times (derived during the surface clutter simulation workflow) to generate a topography-following time domain interval (and corresponding average) velocity model with free space velocity above, and pure water ice velocity below, the surface delay time.
15. Use the average velocity model to convert the 3D migrated volume to depth below the maximum areoid radius datum.
16. Re-datum the depth-converted 3D migrated volume from the maximum areoid radius datum back to the SAR processing datum (areoid+10,118.0 m).

To the extent possible and practical, careful quality control (QC) is performed on the output from all of these steps during the course of processing. As with any multi-step and/or complicated

process, QC is an important part of the 3D methodology to identify/correct unexpected data problems and otherwise ensure the data is progressing as expected through the workflow. For this project, three cases in point are worth mentioning here:

- After Step 4, during routine QC of co-registered radargrams and corresponding surface clutter simulations to evaluate co-registration effectiveness, graphs of derived “raw” co-registration differential time shifts are compared with their applied median-smoothed versions. It was noticed that for some observations acquired after orbit 50,000, the “raw” shifts abruptly become noisier (i.e. exhibit larger frame-to-frame variation) beyond an arbitrary number of frames from the beginning of a given observation. Upon closer scrutiny, the cause was found to be a lateral misalignment between the frames of the radargram and those of the simulation, which in turn stems from the so-called data block counter anomaly (DBCA) where noisy spurious data packets are introduced into the MRO science data stream. The DBCA and its side effects during processing adversely impacts the 3D image.
- It was noticed after Step 11 that the gain variation within interpolated/regularized crossline bin profiles *increased* after compensating the gain levels of the input radargrams for gain changes induced by SA and/or HGA position changes during sounding. This result was the *opposite* of that expected, and thus Step 9 was omitted to forestall any deleterious side effects the increased gain variation might have on subsequent imaging steps. Further investigation as to why this occurred is recommended.
- Also after Step 11, it was noticed within a certain range of interpolated and regularized inline profiles that localized returns, incongruous both in delay time and location compared with the prevailing returns in the profiles, were “marching” across the profiles when panning through their displays, a clear indication of a problem with geometry assignment in the input data. After further investigation, it was determined that a single descending observation (45646-03) was somehow erroneously assigned the geometry of another ascending observation (44901-01) having the same number of frames, leading to improper treatment of the data during processing and manifesting as described above in the interpolated and regularized 3D volume. Because of the added time that would be required to repeat the processing including this single observation after correcting its geometry, it was decided to simply omit the observation for this pilot project and repeat Step 11 for the affected part of the 3D volume. Going forward, an additional automatic check will be made to ensure that geometry information supplied for use in performing 3D processing is consistent with that supplied with the observations after SAR processing.

Results

Figure 2 shows the surface clutter simulation (top) and radargram after delay time co-registration (middle) for observation 7452-02 transecting the DM 3D area. Careful scrutiny and comparison of these “advanced 3D” input products reveal that most of the visible signal in the radargram is in fact surface clutter, with the exception of returns from the base of a debris covered glacier toward the northern end of the observation that don’t appear in the simulation. Returning the surface clutter to locations from whence it came is one of the primary reasons for treating the data collectively in 3D. Superimposing these two displays (bottom) illustrates the effectiveness

of the co-registration process at removing the residual time shifts left in the radargram after SAR processing, with no visible delay time difference in the surface returns between sim and radargram.

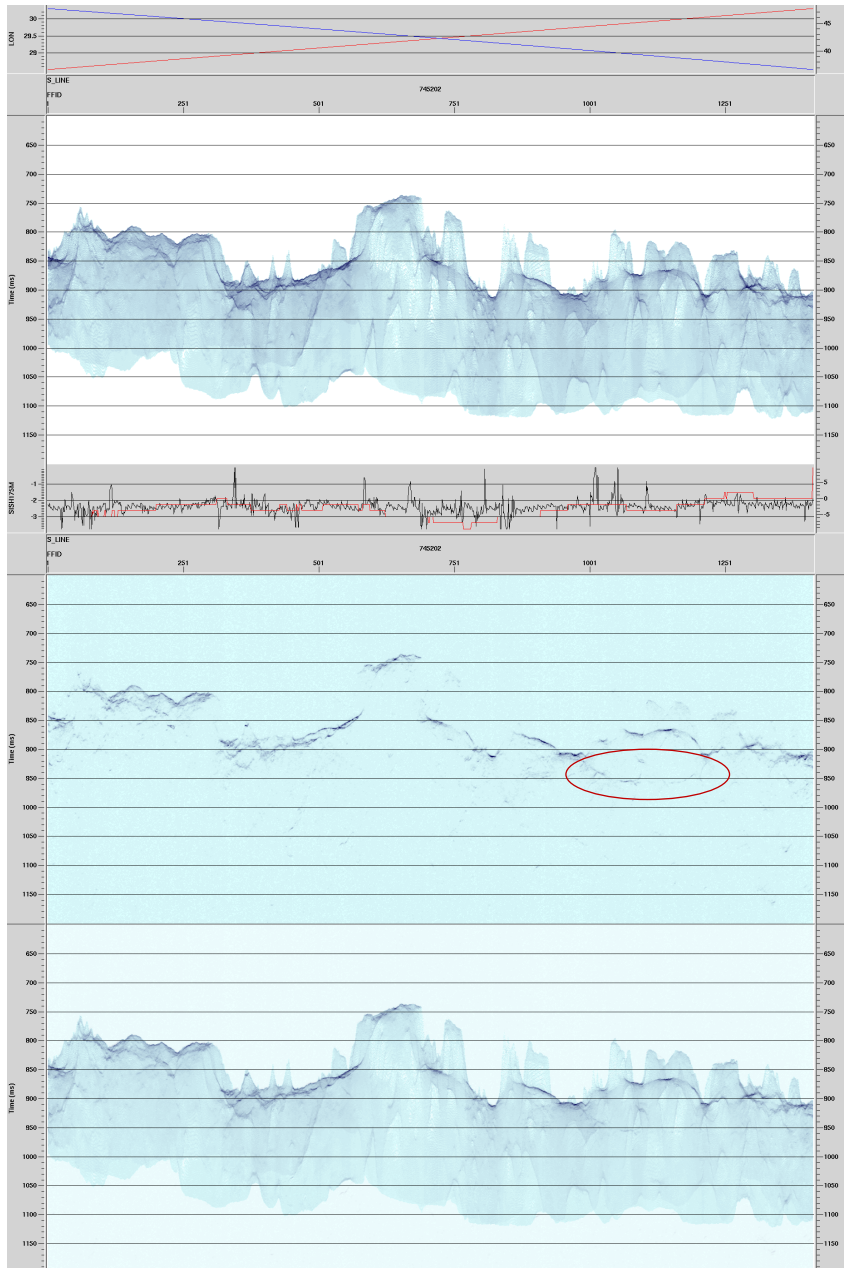


Figure 2. SHARAD observation 7452-02, approx. 653 km long, among 467 observations selected for inclusion in the DM 3D pilot study. Scrutiny and comparison of the surface clutter simulation (top) and co-registered radargram (middle) shows that most visible signal arriving after the surface return is in fact surface clutter except for faint subsurface returns (red oval) interpreted as reflections from the base of a debris covered glacier (DCG). Superimposing the two (bottom) allows for visual assessment of predicted vs. actual first returns alignment. The headboard plot above the simulation shows the frame-by-frame along-track longitude (blue) and latitude (red) while that above the radargram shows the frame-by-frame residual time shifts (red) applied to the radargram to align its first returns with those of the clutter simulation and, in this case, range from around -0.375 to $0.0 \mu\text{s}$ (-10 to 0 range bins). The applied shifts actually result from median smoothing the noisy raw shifts (black) to remove erroneous mis-shifts. Note that both raw and smoothed shifts are integral multiples of the SHARAD range bin size of $0.0375 \mu\text{s}$. Display vertical exaggeration at least 43.5:1 (free space velocity assumption).

Figure 3-Figure 5 show results from the delay time 3D volume after various stages of processing, illustrating the progression in the image after performing the corresponding processing steps. It is clear from examining these results that

3D processing is producing a viable 3D image using the existing SHARAD coverage within the study area even though the coverage in the cross-track direction is not as dense as it should be to prevent aliasing of the wavefield during recording based on the slope magnitudes and orientations in the area. This lack of sufficiently dense cross-track coverage manifests in the 3D image as pervasive lingering processing noise especially noticeable above the first returns in the cross-track profiles after 3D downward continuation and migration.

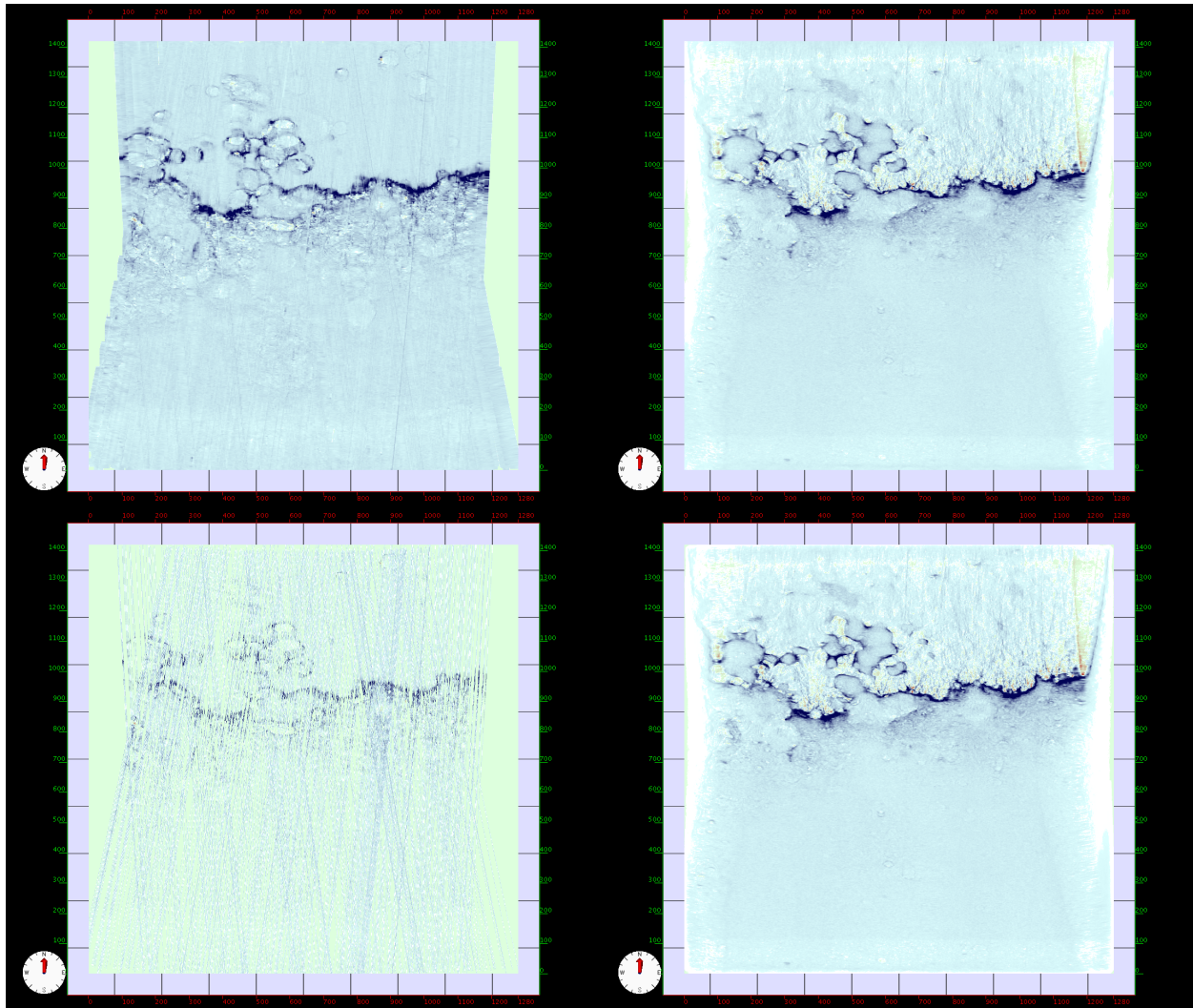


Figure 3. Progression of 3D volume results visualized via a delay time slice at 80.775 μ s taken from the 3D volume after all 2D SAR and preparatory 2D processing through Steps 1-8, 10 (lower left), 3D interpolation and regularization Step 11 (upper left), 3D phase shift downward continuation Step 12, (upper right) and 3D Stolt migration using pure water ice velocity Step 13 (lower right). The lateral dimensions of the project area are ~ 657 km S-N \times ~ 593 km W-E. The delay time reference surface for the time domain volume is the constant radius 3396.097 km, which is the maximum areoid radius found across all frames of all 467 observations used in the project. Note that the downward continued and migrated results are visually identical, which indicates that 1) virtually all of the returns focusing is accomplished by the former and 2) there is only very subtle movement in recorded reflector positioning after migration (note that reflections from steepest slopes likely never recorded).

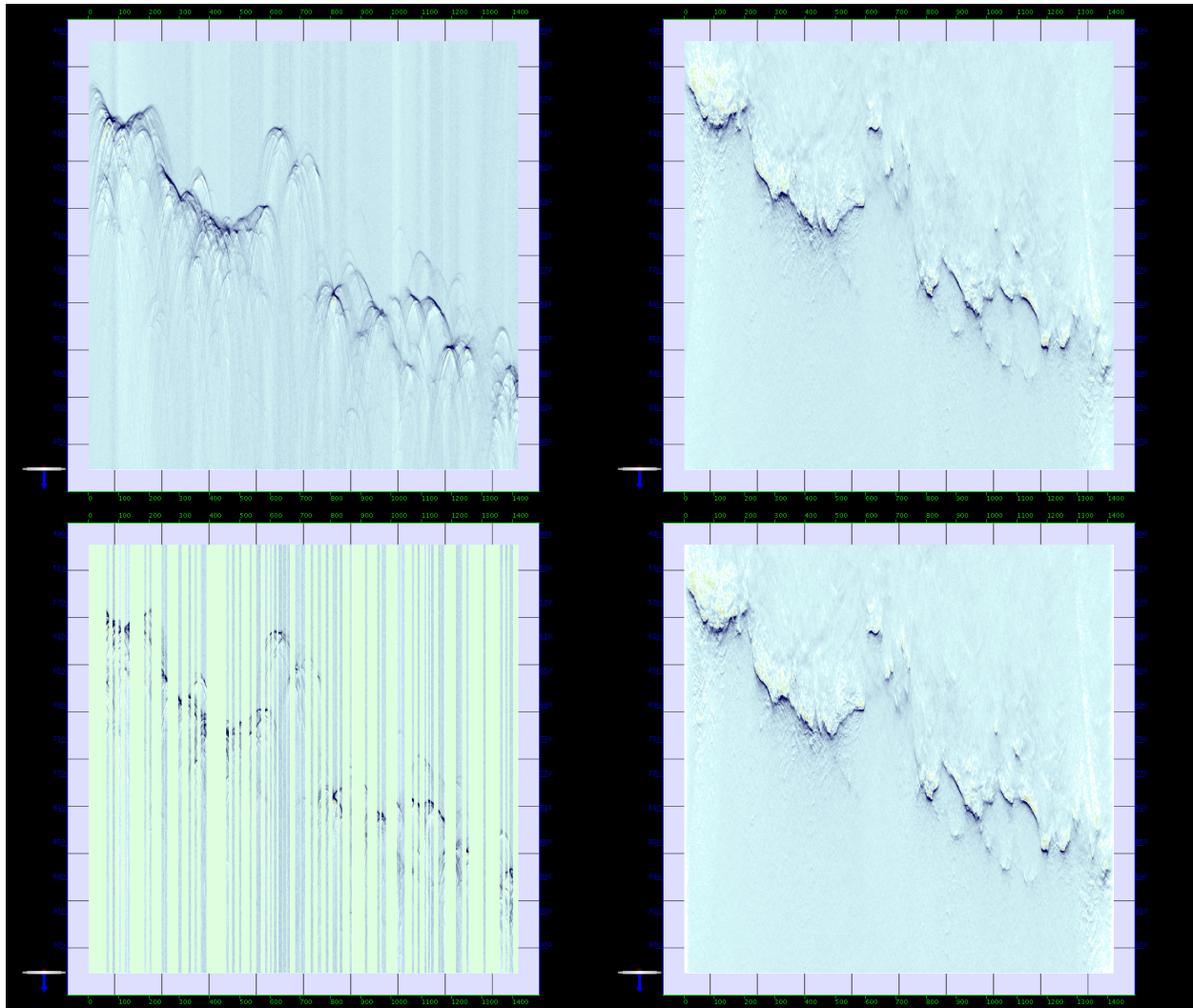


Figure 4. Progression of 3D volume results visualized via a vertical slice at “inline” bin 550 spanning all 1420 “crossline” bins (i.e. S-N profile taken from the 3D volume ~254 km from western boundary of the project area) after 2D SAR and preparatory 2D processing Steps 1-8, 10 (lower left), 3D interpolation and regularization Step 11 (upper left), 3D phase shift downward continuation Step 12 (upper right) and 3D Stolt migration using pure water ice velocity Step 13 (lower right). The delay time window spans 49.9875 to 100.0125 μ s referenced to the constant radius 3396.097 km, which is the maximum areoid radius found across all frames of all 467 observations used in the project. Note that the downward continued and migrated results are visually identical, which indicates that virtually all of the returns focusing is accomplished with the former and there is only very subtle movement in recorded reflector positioning after migration (steepest reflections likely not recorded).

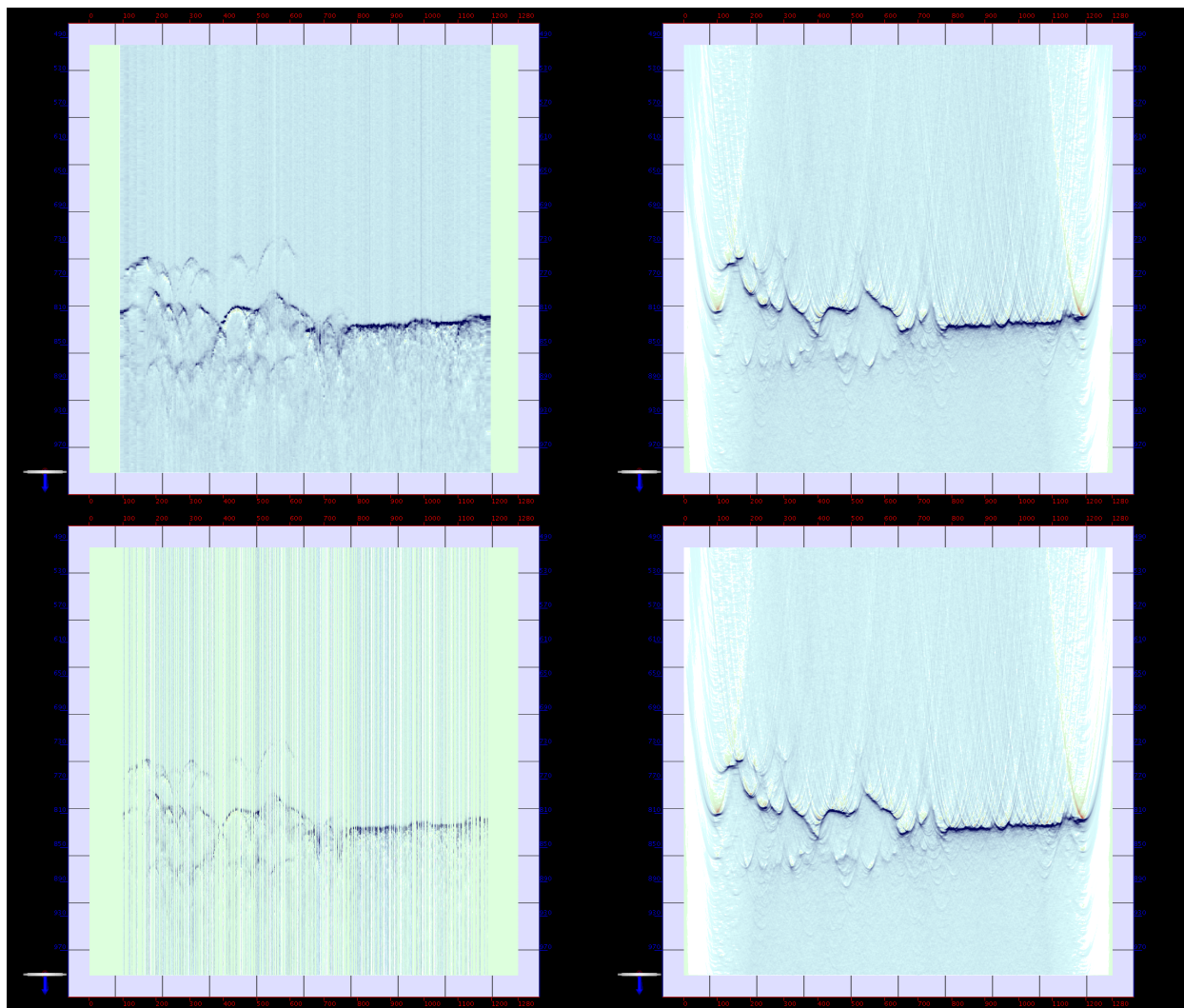


Figure 5. Progression of 3D volume results visualized via a vertical slice at “crossline” bin 1050 spanning all 1280 “inline” bins (i.e. W-E profile taken from the 3D volume ~486 km from southern boundary of the project area) after 2D SAR and preparatory 2D processing Steps 1-8, 10 (lower left), 3D interpolation and regularization Step 11 (upper left), 3D phase shift downward continuation Step 12 (upper right) and 3D Stolt migration using pure water ice velocity Step 13 (lower right). The delay time window spans 49.9875 to 100.0125 μ s referenced to the constant radius 3396.097 km, which is the maximum areoid radius found across all frames of all 467 observations used in the project. Note that the downward continued and migrated results are visually identical, which indicates that virtually all of the returns focusing is accomplished with the former and there is only very subtle movement in recorded reflector positioning after migration (steepest reflections likely not recorded).

Scientific Analysis

The potential for important scientific contributions stemming from use of the DM 3D image, as well as the efficiency with which these contributions can be made, is illustrated by Figure 6 and Figure 7. The cutaway views through the 3D migrated depth image shown in the former may be quickly zoomed as in the latter and, when combined with panning through the various slices in the cutaway, the entire spatial distributions of features of interest may be examined and mapped very rapidly. As of the time of this writing, interpretation and analysis of the delivered 3D image is just beginning. To be complete, any such interpretation and analysis of subsurface features (e.g. lobate debris aprons (LDA), lineated valley fill (LVF), concentric crater fill (CCF) and mantle deposits) delineated by the 3D image must also include a comparison with the analysis of

such features delineated by 2D radargrams and surface clutter simulations. As was the case with the first polar 3D images, since the 3D image produced with this work is the first of its kind in a mid-latitude region, it is important to evaluate the effectiveness, utility and any shortcomings of the 3D image by comparing the imaged features in co-located profiles taken from the 3D image with their “standard” 2D counterparts. The comparison will allow assessment of how imaged features change after 3D vs. 2D treatment, including how the proper treatment of surface clutter clarifies the subsurface picture.

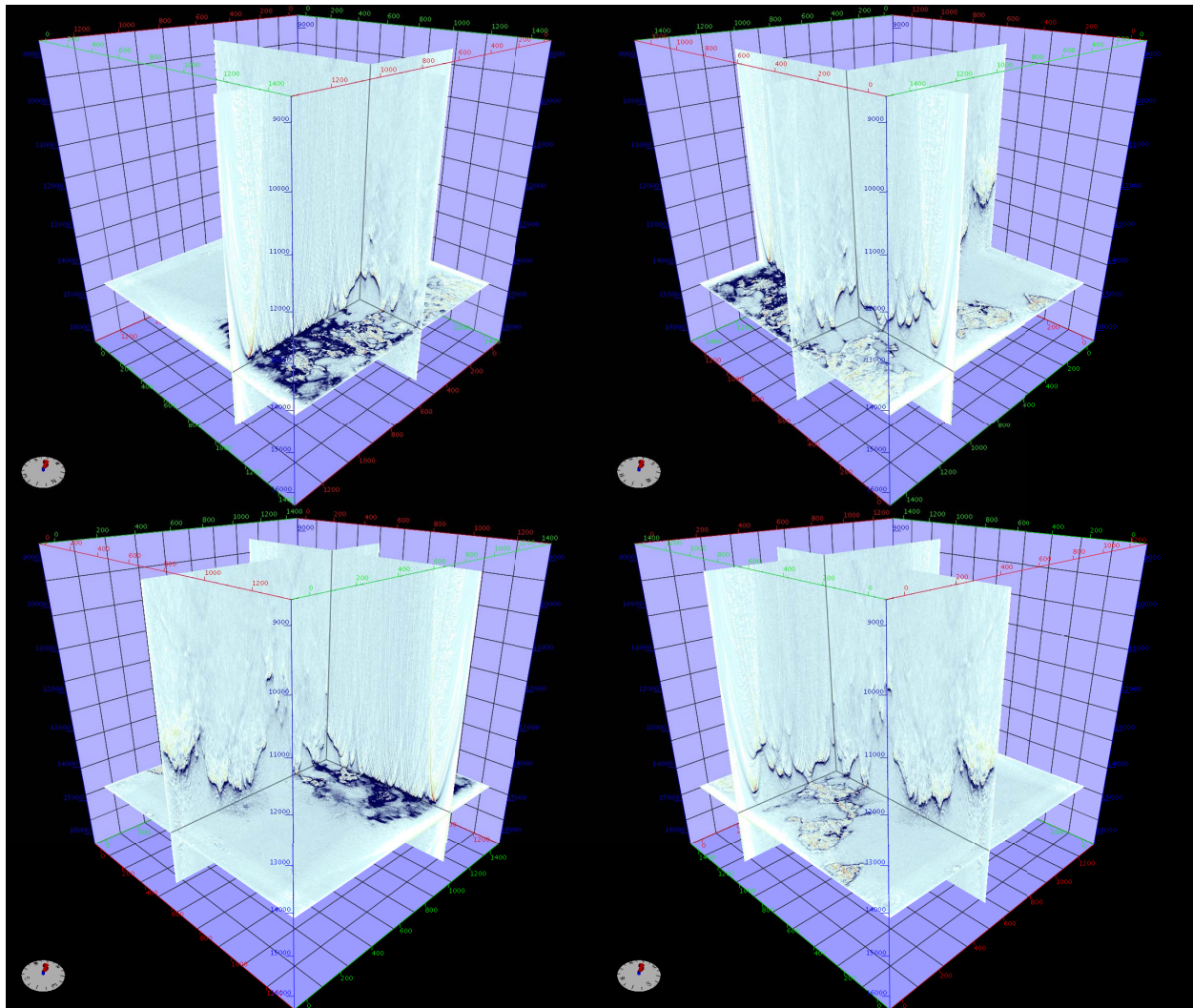


Figure 6. Perspective cutaway views through SHARAD 3D migrated depth image looking (clockwise from lower left) NW, SW, SE, and NE. Display dimensions (S-N distance x W-E distance x thickness) $\sim 657 \times 593 \times 7 \text{ km}^3$, where depth ranges between $\sim 1 \text{ km}$ above and $\sim 6 \text{ km}$ below Mars' areoid. Slices intersect at $\sim (45^\circ \text{ N}, 29^\circ \text{ E}, -4.4 \text{ km})$.

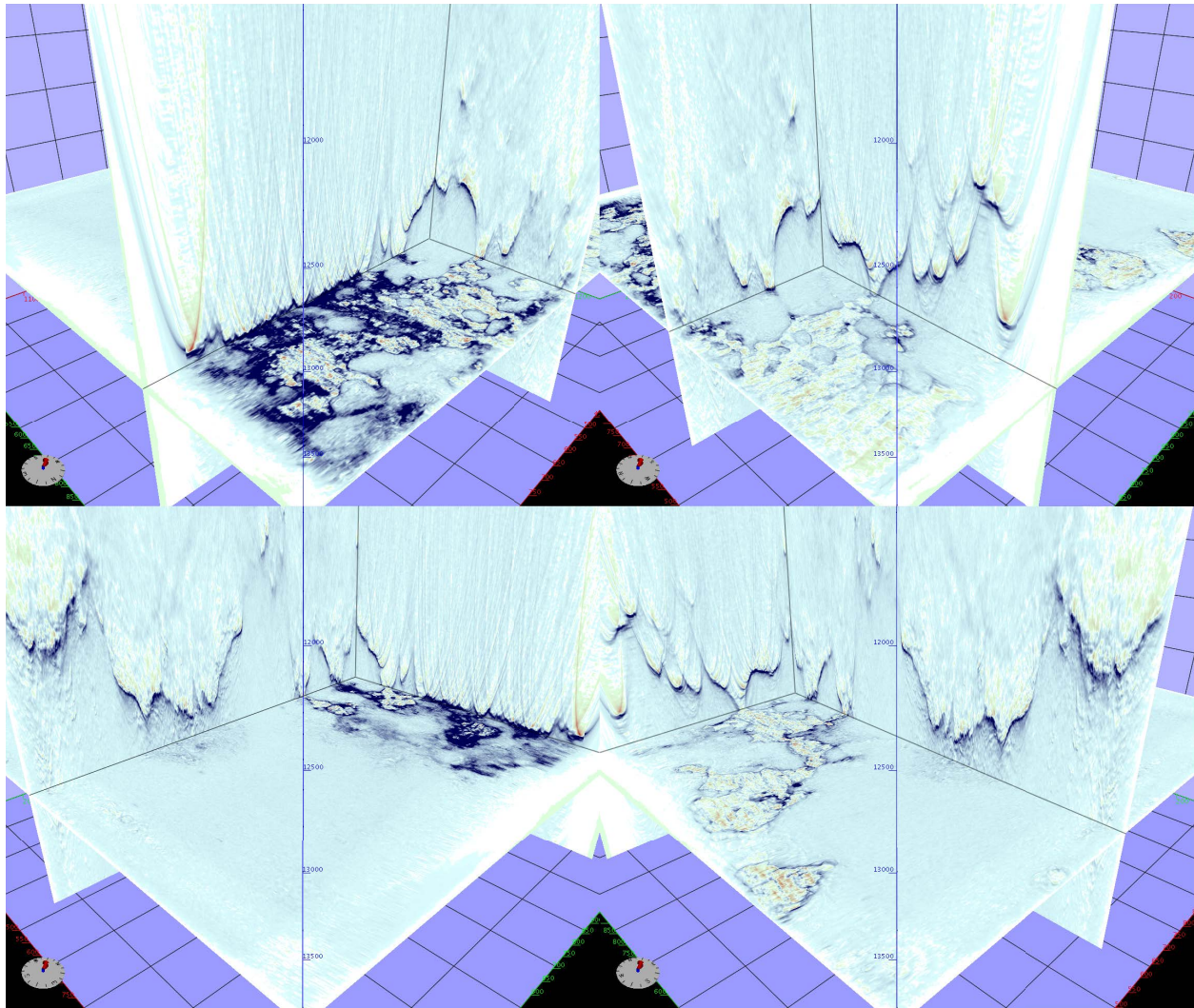


Figure 7. Zoomed perspective cutaway views through SHARAD 3D migrated depth image looking (clockwise from lower left) NW, SW, SE, and NE. Display dimensions (S-N distance x W-E distance x thickness) $\sim 657 \times 593 \times 7 \text{ km}^3$, where depth ranges between $\sim 1 \text{ km}$ above and $\sim 6 \text{ km}$ below Mars' areoid. Slices intersect at $\sim (45^\circ \text{ N}, 29^\circ \text{ E}, -4.4 \text{ km})$.

Estimated vs. Actual Project Duration and Scope

The tasks proposed for the DM 3D pilot study were estimated to take 5.5 weeks whereas they actually took 19.3 weeks to complete (referring to the list of processing steps):

- 8.0 weeks to perform Steps 1 and 2.
- 3.0 weeks to perform Steps 3 – 5.
- 8.3 weeks to perform Steps 6 – 16.

The extra time required to complete the work was mainly due to demands for time from other projects, as well as some unforeseen technical problems that required additional time to evaluate and solve (e.g. see the previous discussion on QC during processing).

Additionally, the proposed DM 3D pilot study scope included producing a 3D image from the surface clutter simulations, however, the proposed project budget overlooked the time and expense required for this task and therefore wasn't completed. Moreover, it became imperative to set aside continued work on the DM 3D pilot study in favor of the ongoing PB "advanced" 3D project due to pressing remaining tasks and time constraints of the latter.

Recommendations for Continued 3D Processing Work

To build on the work done thus far in this DM 3D pilot study, we recommend generating a 3D surface clutter image using the processing workflow described herein (the simulations are already available within the processing system). Also, because of the cross-track coverage deficiency, the bilinear 3D interpolation and regularization method, while simple and tolerant of non-uniform spatial sampling, falls short of properly interpolating steeper slopes in the data across large coverage gaps, which then contributes to generating imaging operator artifacts in the 3D image (particularly visible in the crossline views of Figure 5). We recommend that alternative 3D interpolation and regularization methods be investigated and tested to find one more tolerant of the cross-track structural under-sampling in the 3D volume. Finally, we recommend testing two additional 3D migration methods, one that admits vertically interval velocity variations and one that further admits lateral velocity variations.

Participants and Acknowledgements

The DM3D pilot study is a collaboration among scientists and researchers at Freestyle Analytical & Quantitative Services (FREAQS), LLC, Planetary Science Institute (PSI), and Smithsonian Institute (SI). This work was funded by NASA's Mars Reconnaissance Orbiter (MRO) mission. The surface clutter simulator was provided by University of Arizona. The data processing was accomplished in part using Halliburton Landmark's SeisSpace® ProMAX® 3D data processing system. The 3D volume interpretation and analysis is to be done in part using SeisWare™ data interpretation system. Beyond the DM3D pilot study contributors from various institutions, we would like to acknowledge Dr. Stewart A. Levin of Stanford University for the SeisSpace® ProMAX® 3D downward continuation module written and used for prior and this SHARAD 3D work.

References

Campbell, B.A. et al., 2021 (to appear in Icarus). Calibration of Mars Reconnaissance Orbiter Shallow Radar (SHARAD) Data for Subsurface Probing and Surface Reflectivity Studies.

Choudhary, P., Holt, J.W., and Kempf, S.D., 2016. Surface Clutter and Echo Location Analysis for the Interpretation of SHARAD Data From Mars. IEEE Geoscience and Remote Sensing Letters, vol. 13, no. 9, pp. 1285-1289, doi: 10.1109/LGRS.2016.2581799.

Foss, F.J., II, 2018. 3-D Processing and Analysis of MRO SHARAD Data Acquired Over Mars' South Polar Layered Deposits, Project Report, publicly available via <https://sharad.psi.edu/3D/reports/PA3D/Foss%20Project%20Report/SPLD%203D%20Project%20Report.pdf>

Foss, F.J., II, Putzig, N.E, Campbell, B.A., and Phillips, R.J., 2017. 3-D Imaging of Mars' Polar Ice Caps Using Orbital Radar Data. *The Leading Edge* 36, 43-57, doi:10.1190/tle36010043.1. Public access via <https://www.ncbi.nlm.nih.gov/pmc/articles/PMC5791158>

Foss, F.J., II, 2016. 3-D Processing and Analysis of MRO SHARAD Data Acquired Over Mars' North Polar Layered Deposits, Project Report, publicly available via <https://sharad.psi.edu/3D/reports/PB3D/Foss%20Project%20Report/NPLD%203D%20Project%20Report.pdf>

Putzig, N.E. et al., 2018. Three-dimensional radar imaging of structures and craters in the Martian polar caps. *Icarus* 308, 138-147, doi:10.1016/j.icarus.2017.09.023.

Putzig, N.E., 2015. Advanced 3-D Subsurface Imaging and Analysis of Planum Boreum with SHARAD Data. Scientific/Technical/Management portion of MDAP proposal, publicly available via https://sharad.psi.edu/3D/reports/PB3Dv2/Putzig_MDAP_2015_STM.pdf